

Energy-Efficient Active Element Selection in RIS-aided Massive MIMO Systems

Wilson Souza Jr, Taufik Abrão, José Carlos Marinello

Abstract

This paper delves into the critical aspects of optimizing energy efficiency (EE) in active reconfigurable intelligent surface (RIS)-assisted massive MIMO (M-MIMO) wireless communication systems. We develop a comprehensive and unified theoretical framework to analyze the boundaries of EE within M-MIMO systems integrated with active RIS while adhering to practical constraints. Our research focuses on a formulated EE optimization problem aiming to maximize the EE for active RIS-assisted M-MIMO communication systems. Our goal is strategically finding the number of active RIS elements for outperforming the EE attainable by an entirely passive RIS. Besides, the proposed novel solution has been specifically tailored to the innovative problem considered. The formulation and solution design take into account analytical optimization techniques, such as lagrangian dual transform (LDT) and fractional programming (FP) optimization, facilitating the effective implementation of RIS-aided M-MIMO applications in real-world settings. In particular, our results show that the proposed algorithm is able to provide up to 120% higher EE in comparison to the entirely passive RIS. Besides, we found that the active RIS can operate with lower than half of reflecting elements with respect to the entirely passive RIS. Finally, in view of active RIS achieving the complete utilization of amplification power available, it should be equipped with a reasonable number of reflecting elements, above $N = 49$.

Index Terms

RIS element selection; Energy efficiency (EE); Massive MIMO (M-MIMO); Spectral efficiency; Reconfigurable intelligent surface (RIS); Heuristic evolutionary optimization; Convex optimization.

I. INTRODUCTION

The proliferation of the fifth generation (5G) wireless network has catalyzed worldwide incentive and development efforts in research, resulting in an intensified exploration of possibilities offered by the sixth generation (6G) wireless network. Projected to be characterized and recognized by exceptional data-driven capabilities and instantaneous connectivity global ubiquity, 6G is expected to provide a wide range of applications and services that will revolutionize communication systems. These innovations span across diverse domains, such as extended reality (XR), holographic communications, etc., promising to redefine the technological scenario. The advent of 6G will bring forth plenty of new services and withal elevate existing ones to higher levels. However, in view of reaching this aim, the integration of cutting-edge technologies becomes essential to facilitate the deployment of these services and ensure their optimal functioning in the technological scenario. In essence, the commercialization of 6G will necessitate a proactive approach in adopting state-of-the-art technologies, marking a paradigm shift in how we envision wireless communication networks' potential.

Among all emerging technologies, RIS stands out as one of the most promising recent enabling techniques poised to revolutionize future communication systems, extending beyond the 5G and 6G eras. RIS has the potential to significantly enhance transmission capabilities by establishing a "virtual" reconfigurable/re-programmable communication link. Essentially the RIS, is a thin planar surface consisting of a massive number of low-cost reflecting elements composed of meta-materials, to reconfigure and redirect the impinging signal, by changing its electromagnetic properties (phase and/or magnitude) [1], so

J. C. Marinello is with the Electrical Engineering Department, Federal University of Technology PR, Cornélio Procópio, PR, Brazil. (e-mail: faugustobueno@gmail.com, omluizalberto@gmail.com, jcmarinello@utfpr.edu.br).

Wilson Souza Jr and T. Abrao are with the Department of Electrical Engineering Londrina State University, Parana Brazil (e-mail taufik@uel.br)

that, the reflected signal can be focused toward a specific direction with a specific gain. The electromagnetic properties of the impinging waves are precisely controlled by utilizing electronic components such as PIN diodes or radio frequency (RF) switches integrated into the RIS panel. For instance, changing the impedance of PIN diodes or tuning the RF switch facilitates the manipulation of the reflection with respect to its direction and amplitude, respectively. This dynamic adjustment serves to enhance specific target metrics. Therefore, RIS is promising due to its capacity to control in a software-defined manner the wireless environment and its potential to mitigate certain intrinsic effects. The specific advantages of the RIS arrays can be summarized as follows [2]:

- 1) Easiness in implementation;
- 2) spectral efficiency (SE) and EE enhancement;
- 3) Sustainability;
- 4) Compatibility.

Due to the aforementioned characteristics, RISs are recognized as a potential solution for solving a wide range of challenges in commercial and civilian applications. Besides, in contrast to conventional relaying methods such as Amplify-and-Forward (AF) and Decode-and-Forward (DF), RIS presents many advantages. It offers a cost-effective yet efficient solution that optimizes both system's EE and SE. On this matter, like any emerging technology, new applications and a range of problems arise as a result. Besides, from the perspective of communication and signal processing, open problems such as phase-shift optimization of scattering elements, and channel acquisition of additional links imposed by deploying the RIS are extremely necessary to be addressed and efficiently solved.

Although RIS presents a range of advantages, there are some critical issues that are found in real-world applications. Consequently, various architectural variants for the RIS have been introduced to address these challenges and enhance its overall effectiveness. These variations aim to significantly enhance performance, offering innovative solutions to overcome challenges and elevate the effectiveness of RIS-supported communication systems. Among them, we can remark the active RIS structure, which is an alternative for providing better conditions for the double-fading attenuation link. In active RIS, each reflecting element is supported by a set of active-load impedances that enable the active RIS to operate as an active reflector reflecting and applying power amplification on the impinging signal. An interesting advantage of the active RIS elements is their capability to estimate the channel between the transmitter-RIS in downlink (DL) and uplink (UL) at the RIS side [3]. Besides, since the active RIS has the ability to amplify the incident signal, fewer reflecting elements are required to achieve the same signal-to-noise ratio (SNR) at the receiver when compared with the conventional entirely passive RIS [4]. However, evaluating the EE for the entirely passive RIS versus active RIS is an important problem that should be further investigated.

Conversely, the proliferation of M-MIMO technology, characterized by the deployment of an extensive array of transmit/receiver antennas at base station (BS), plays a pivotal role in enhancing the SE of the system. This technology is instrumental in efficiently accommodating multiples user's equipments (UEs) by leveraging the same physical resources. This strategic utilization enhances the SE and optimizes the resource utilization, exemplifying the versatility and efficiency of M-MIMO in contemporary wireless communication systems.

Besides the aforementioned technologies, a promising technology to be present in future communications networks is the millimeter-wave (mmWave) technology. It emerges as a strategic pivotal solution in addressing the evolving connectivity demands. Operating within the high-frequency spectrum, typically spanning from 30 to 100 GHz, mmWave technology presents a promising solution capable of supplying characteristics such as the utilization of higher bandwidth for contemporary communication networks. Furthermore, with the large arrays, the near-field emerges, enabling the beam focusing instead of the traditional beam steering for far-field communications [5]–[7].

However, the implementation of these higher-frequency systems, which often entails the use of large-scale arrays at the BS or the RIS, introduces inherent complexities in both passive and active beamforming, demanding low-complexity, approximate yet efficient solutions for accurate channel estimation and RIS

configuration. The joint operation of RIS, M-MIMO, and mmWave technologies emerges as key enablers for future communication systems. Expected to play central roles in the upcoming generation of wireless networks, these technologies are designed to support high data rates and accommodate a substantial number of connected UEs, operating with expanded array sizes. In response to this evolution, there is a fundamental growth to prioritize the system's EE, measured in bits-per-Joule¹, as a crucial performance metric. The focus on EE emphasizes the matter of developing sustainable communication systems, especially as efficient energy utilization becomes a global concern across various fields, including telecommunications. In function of alarming levels of climate change, there is an urgent need to limit global warming to 1.5 degrees above the pre-industrial mark [8]. Within this context, the development of the next-generation telecommunication standard, often referred to as Beyond-5G (B5G) or 6G, assumes particular importance. It aims to establish a highly energy-efficient system capable of meeting expected requirements, such as a peak throughput of 1 [Tbps] and latency in the order of microseconds [9]. This forward-looking approach aligns with the broader goal of enabling technological advancements that not only meet the requirements necessary in terms of performance but actively contribute to the sustainability challenges of our time.

In light of these challenges, the development of pioneering strategies that not only enhance EE but also facilitate the intricate processes of channel estimation and configuration for large-scale array systems is of paramount importance. In this paper, our focus stays dedicated to addressing these challenges with innovative approaches and practical solutions tailored to the modern network's infrastructures.

A. Contributions of the paper

The contributions of this paper lie in analyzing the RIS-assisted M-MIMO scenario, which will become essential components of future communication systems. Specifically, the aim is to devise a solution that effectively optimizes the signal amplification of active RIS concerning the EE, envisaging the determination of the number of active RIS elements that outperforms entirely passive RIS. Elaborate further, in this paper, we systematically:

- Propose a comprehensive optimization methodology for system EE maximization, focusing on the deployment of specific optimization tools, including convex optimization procedures in view of reducing the computational complexity aiming the application of the algorithm in a real-world scenario;
- Optimize the phase and amplitude of the active RIS in a sustainable perspective, *i.e.*, the phase and amplitude that results in the power consumption necessary to obtain high-performance gains sufficient to outperform the totally passive RIS;
- Investigate the number of RIS active elements to be selected that surpasses the EE performance of the entirely passive RIS within the system EE optimization framework and different configurations/scenarios parameters.

B. Organization

The remainder of this paper is organized into seven sections. These sections are meticulously structured to provide a comprehensive exploration of the various aspects of the RIS-assisted M-MIMO system. In **Section II**, we summarize the related works; while in **Section III**, we present the groundwork by formulating a general system model that effectively captures the key aspects associated with the integration of the active RIS into the M-MIMO systems. Also, we explore the SE and EE definitions and present the coupling power consumption model for RIS-assisted M-MIMO systems. In **Section IV**, we review the definitions, features, and concepts of some fundamental techniques for addressing our intended problem, such as FP techniques and sum-of-ratio techniques. Moving forward, in **Section V**, we meticulously present the defined problem formulation, emphasizing its relevance and significance in contemporary real-world applications. The motivations and justifications for adopting this particular problem are thoroughly

¹Alternatively, Joule-per-bit.

expounded, shedding light on the specific challenges and opportunities that emphasize its importance in modern communication systems. **Section VI** provides a complete and detailed description of our proposed solution for the EE problem in active RIS-assisted M-MIMO systems. **Section VII** presents numerical results, accompanied by an extensive and in-depth discussion on the effectiveness, efficiency, and potential of the proposed technique. The section also includes a relevant discussion on the advantages/drawbacks of the active RIS structure in contrast to the entirely passive RIS within the context of EE.

Finally, in **Section VIII**, we provide a relevant and comprehensive discussion that encapsulates our perspective into the problem-solving approach adopted throughout this paper as well as the obtained insights. Our analysis and conclusions are framed within the broader context of the current state of the art, aiming to provide valuable insights and potential directions for future research.

II. RELATED WORKS

An extensive number of works including [13]–[30] have studied the RIS deployment impact in M-MIMO systems under different objectives, such as: maximizing the weighed sum-rate (WSR) [13], [14], maximizing the sum-rate (SR) [15], maximizing the EE [16]–[18], RIS-assisted sensing [19], [20], minimizing the total transmit power [21], maximizing the minimum rate [22], [23], for interference nulling [24], [25], and active RIS [26]–[30].

The above-cited studies demonstrate the immense potential and versatility of RIS within wireless systems. The work in [13] investigates the weighted SR maximization. It uses a convex optimization approach to design the BS precoding matrix and the RIS-phase shift for the passive RIS. The paper proposes two different techniques for the analyzed problem. The proposed optimization method utilizes FP techniques aiming at the problem "convexation". Besides, an block coordinate descent (BCD) method is utilized to optimize sequentially the BS precoding matrix and the RIS phase shift, where analytical methods and *Riemannian* conjugate gradient have been utilized. The proposed method is available under two different scenarios: perfect and imperfect channel estimation. Numerical simulations confirm the effectiveness and efficiency of the proposed method.

The work in [14] suggests that by attempting to reduce inter-cell interference, the weighted SR in RIS-aided DL multicell could be maximized. Hence, to achieve this aim, [14] jointly optimizes the active precoding matrices at BSs and the phase shifts at the RIS subject to each BS's power constraint and unit modulus constraint, respectively. In this case, the optimization problem does not consider any Quality of Service (QoS) restriction, *e.g.*, a minimum rate requirement for the users. As a result, this solution tends to maximize the rate of users with better channel conditions.

In [15], the authors investigated the ergodic rate of an RIS-assisted M-MIMO system. Applying random matrix theory, the authors derive a closed-form lower bound expression for the system ergodic rate. The derived bound reveals tightness over several system and channel parameters. Besides, it is promising since the statistical channel state information (CSI) optimization can be deployed based on this bound, being useful to alleviate the channel estimation burden since it matches very well with the expected results. Besides, they provided a gradient-ascent method to optimize the RIS angle phase shift in view of maximizing the system SR.

The EE maximization problem is addressed in [16] by considering UL multi-user single-antenna devices and Multiple-input single-output (MISO) RIS-aided systems. The joint optimization involves the transmit power at users, phase shift at the RIS, and combining matrix at BS receiver. The proposed BCD iterative procedure can handle one variable during each iteration while the others are held fixed. Numerical results indicate that the proposed scheme outperforms baselines that jointly optimize two of three variables.

In [17], the joint number of antennas, power allocation, and passive RIS reflecting coefficients optimization for EE maximization with statistical CSI is studied. Analytical techniques have been applied in view of maximizing the EE with low overhead for channel estimation. EE problem has been maximized with a low-complexity algorithm, where the power allocation, RIS phase shift, and the number of active antennas at BS have been optimized based on closed-form expressions, utilizing BCD method. The method was

demonstrated to be promising, outperforming the gradient ascend methodology for passive RIS reflecting coefficients optimization with statistical CSI.

In [18], the authors also analyzed the EE in RIS-assisted systems. In this study, the EE maximization has been analyzed under joint optimization of power consumption for both RIS and BS. The authors proposed an innovative power consumption model on the RIS by considering the ON and OFF state of RIS unit reflecting element, matching further precisely with the real-world behavior of physical components. The paper also proposes low-complexity and effective algorithms, which have been proven by the simulation results to be promising.

In [19], the authors studied the integrated sensing and communication (ISAC) system for a double RIS-assisted system. The research primarily focuses on addressing the challenge of mutual interference between the radar and communication functionalities by leveraging a joint optimization approach for beamforming and radar operations. To manage the complexity of the solution, the authors introduce a penalty dual decomposition (PDD)-based approach and a BCD algorithm. These methods effectively reduce computational complexity, offering practical and efficient solutions for real-world implementation. Moreover, the work presented in [20] addresses the challenges of a sensing-assisted multi-user mmWave system. The study focuses on optimizing the channel sensing duration for each UE to enhance the overall system SR. By effectively managing the sensing duration, the research aims to improve the performance of the mmWave system, offering potential advancements for future wireless communication technologies.

In [21], the phase shift and BS beamforming optimization techniques have been proposed in view of minimizing the UL transmit power in an RIS-aided Internet of Things (IoT) network. The proposed technique was demonstrated to be promising since it can reduce to about half of the UL transmit power over the conventional scheme without RIS. The methodology exploits the product *Riemannian manifold* structure of the sets of unit-modulus phase shifts and unit-norm beamforming vectors. Besides, the *manifold* method converts the non-convex UL transmit power minimization problem into an unconstrained problem and then finds the optimal solution over the product *Riemannian manifold*.

In [22], the focus was on the study of the maximum-minimum rate problem. The research delved into the joint optimization of transmit and passive beamforming, considering the uncertainty of UEs locations. To address this challenge, the authors proposed an alternating optimization approach combined with successive convex approximation (SCA) technique and a penalty algorithm employing a double loop.

In the research paper [23], the authors demonstrated that the non-convex max–min rate problem in RIS-assisted multi-user communication systems can be reformulated into a second order conic programming (SOCP) problem. They also explored the application of semi-defined relaxation (SDR) and SCA techniques to optimize the passive and active beamforming for the system under consideration.

In [24], the RIS structure is deployed aiming at interference nulling, where an alternating projection method is utilized. This method is able to converge for a solution that completely eliminates the interference. However, the number of elements for achieving this goal can vary according to some parameters, such as the number of served UEs. Besides, the authors also explored the max–min rate problem. The numerical results are revealed to be promising since the proposed procedure achieves high performance with low complexity. Adhering to a similar approach, the authors in [25] proposed a method to determine the angles for two distinct passive RISs, aiming to achieve complete orthogonalization of channels between UEs and thereby nulling interference. The investigation delves specifically into both diagonal and beyond-diagonal RISs, employing a *Manifold*-based algorithm to find the angles for both RISs, adhering to the unitary matrix constraint essential for achieving complete orthogonalization of channels between the UEs. Notably, the study highlights that signal amplification is unnecessary for achieving orthogonalization. Furthermore, the paper introduces an efficient channel estimation method to complement the proposed approach.

Our previous related works and contributions on the resource efficiency (RE) optimization, EE and SE in M-MIMO systems aided or not by RIS include: [17], [31]–[39]. In this paper, we propose to deploy the FP methodology to solve the phase-shift and amplification coefficients of an active RIS aiming to EE maximization problem considering the context of the DL RIS-aided multiuser M-MIMO systems.

III. GENERAL SYSTEM MODEL FOR RIS-AIDED M-MIMO

We start the section by describing the general model for M-MIMO systems assisted by an RIS setup considered. This system model is conceived to cover a diverse range of practical scenarios. Subsequently, we present the models for the DL received baseband signals. Built such model, we finish the section by formulating expressions for SE and EE within the specified RIS-aided M-MIMO scenarios. The notation deployed in this paper is entirely outlined in Table I.

TABLE I
LIST OF NOTATION AND SYMBOLS FOR THE RIS-AIDED M-MIMO SCENARIO

Symbol	Description
$M \in \mathbb{Z}_+$	Number of BS antennas
$K \in \mathbb{Z}_+$	Number of UEs
$N \in \mathbb{Z}_+$	Number of total RIS elements
$\mathcal{K} = \{1, 2, \dots, K\}$	UEs set
$\mathcal{N} = \{1, 2, \dots, N\}$	RISs elements set
$\lambda > 0$	Carrier wavelength
$\beta_1 \in \mathbb{R}$	Large-scale fading coefficient of the channel from BS to RIS
$\beta_{2,k} \in \mathbb{R}$	Large-scale fading coefficient of the channel from RIS to k -th UE
$\mathbf{H} \in \mathbb{C}^{M \times K}$	Cascaded channel matrix of the BS and UEs through RIS
$\mathbf{H}_1 \in \mathbb{C}^{M \times N}$	Channel between the BS and RIS
$\bar{\mathbf{H}}_1 \in \mathbb{C}^{M \times N}$	Line-of-sight (LoS) component of the BS and RIS channel
$\hat{\mathbf{H}}_1 \in \mathbb{C}^{M \times N}$	Multipath component of the BS and RIS channel
$\mathbf{H}_2 \in \mathbb{C}^{N \times K}$	Channel between the RIS and UEs
$\bar{\mathbf{H}}_2 \in \mathbb{C}^{N \times K}$	LoS component of the RIS and UEs channel
$\hat{\mathbf{H}}_2 \in \mathbb{C}^{N \times K}$	Multipath component of the RIS and UEs channel
$\mathbf{v} \in \mathbb{C}^N$	RIS amplitude/phase-shift vector
$\Phi \in \mathbb{C}^{N \times N}$	RIS amplitude/phase-shift diagonal matrix
$\kappa_1 \in [0, \infty)$	Rician κ -factor for RIS and BS channel
$\kappa_{2,k} \in [0, \infty)$	Rician κ -factor for RIS and k -th UE
$p_k \in \mathbb{R}^+$	Power designated to the k -th UE
$\mathbf{W} \in \mathbb{C}^{M \times K}$	Precoding matrix
$s_k \in \mathbb{C}$	Information symbol intended to the k -th UE
$n_k \in \mathbb{C}$	additive white gaussian noise (AWGN) sample at the k -th UE
$\mathbf{z} \in \mathbb{C}^{N \times 1}$	AWGN sample vector at the RIS
$\alpha_n \in \mathbb{R}_+$	Amplitude value of n -th element of RIS
$\theta_n \in [0, 2\pi)$	Phase-shift value of n -th element of RIS
$\alpha_{\max} \in \mathbb{R}_+^*$	Maximum amplitude provided by the RIS
$P_{\max}^{\text{RIS}} \in \mathbb{R}_+$	Maximum amplification power of RIS

Consider a DL RIS-assisted M-MIMO scenario where the direct link between the BS and UEs is completely obstructed, thus, K single antenna UEs are served by the BS with M elements through an RIS with N elements. Besides, we assume a direct connection between the RIS and the BS is made by means of a dedicated link via a programmable controller, enabling the BS to manage both phase shifts and amplitude coefficients of the RIS. Furthermore, we assume that the time necessary for RIS amplitude/phase configuration is shorter than the channel *coherence time*, *i.e.*, at the start of each time slot, the BS should configure the RIS appropriately for its operation. Let us denote \mathbf{H}_1 as the channel from the BS to the RIS and \mathbf{H}_2 as the channel from the RIS to the UEs. The cascaded channel between the BS and UEs through the RIS can be given as $\mathbf{H} = [\mathbf{h}_1, \mathbf{h}_2, \dots, \mathbf{h}_K]$; more specifically, denoted as

$$\mathbf{h}_k = \mathbf{H}_1 \Phi \mathbf{h}_{2,k}, \quad \forall k \in \mathcal{K}, \quad (1)$$

where $\Phi = \text{diag}(\mathbf{v}) \in \mathbb{C}^{N \times N}$, with $\mathbf{v} = [v_1^*, v_2^*, \dots, v_N^*]^H \in \mathbb{C}^{N \times 1}$, being $v_n = \alpha_n e^{j\theta_n} \in \mathbb{C}$ the phase-shift and amplitude applied by the n -th element of the RIS, with $\alpha_n \in [0, \alpha_{\max}]$ and $\theta_n \in [0, 2\pi)$. The BS uses a precoding matrix $\mathbf{W} = [\mathbf{w}_1, \mathbf{w}_2, \dots, \mathbf{w}_K] \in \mathbb{C}^{M \times K}$, with $\|\mathbf{w}_k\|^2 = p_k \in \mathbb{R}^+$, in view of beamforming the signal towards the UEs, where p_k is the power allocated for the k -th UE served. Here, for simplicity, we adopt maximum ratio (MR) precoding with equal power allocation (EPA).

Utilizing the system model explained above, the DL baseband transmitted signal $\mathbf{x} \in \mathbb{C}^{M \times 1}$ can be written as

$$\mathbf{x} = \sum_{k=1}^K \mathbf{w}_k s_k, \quad (2)$$

where s_k is the symbol intended to the k -th UE, with $\mathbb{E}[|s_k|^2] = 1$. While the received signal by the k -th UE is given as

$$y_k = \mathbf{w}_k^H \mathbf{h}_k s_k + \sum_{j=1, j \neq K}^K \mathbf{w}_j^H \mathbf{h}_k s_j + \mathbf{h}_{2,k}^H \Phi \mathbf{z} + n_k, \quad (3)$$

in which $n_k \in \mathbb{C}$ is the AWGN sample at the k -th UE, following $n_k \sim \mathcal{CN}(0, \sigma^2)$, $\forall k \in \mathcal{K}$, and $\mathbf{z} \in \mathbb{C}^{N \times 1}$ is the AWGN at the RIS, with $\mathbf{z} \sim \mathcal{CN}(\mathbf{0}_N, \sigma_{\text{RIS}}^2 \mathbf{I}_N)$.

A. RIS-aided M-MIMO Channel Modelling

The RIS takes the form of a thin uniform squared planar array (USPA), featuring $N = N_h \times N_v$ total elements, where $N_h = N_v = \sqrt{N}$ elements in the horizontal and vertical directions, with \sqrt{N} being a positive integer ($\sqrt{N} \in \mathbb{Z}_+$). Furthermore, the elements are vertically and horizontally equally spaced with spacing d_R . Besides, the BS is assumed to be equipped with a uniform linear array (ULA) of M total elements disposed in the x axis, *i.e.*, parallel to the RIS.

In the channel model for RIS-aided M-MIMO, we make the assumption of far-field wavefront propagation regime between the BS and the RIS panels, as well as between the RIS and the UEs, *i.e.*, the planar wavefront is assumed in both links.

BS-RIS link: to be more specific, we establish the channel between the BS and the RIS based on the Rician-fading model, given by [40]–[42]:

$$\mathbf{H}_1 = \sqrt{\frac{\beta_1 \kappa_1}{\kappa_1 + 1}} \bar{\mathbf{H}}_1 + \sqrt{\frac{\beta_1}{\kappa_1 + 1}} \tilde{\mathbf{H}}_1, \quad (4)$$

where $\bar{\mathbf{H}}_1 \in \mathbb{C}^{M \times N}$ corresponds to the deterministic LoS channel component, $\tilde{\mathbf{H}}_1 \in \mathbb{C}^{M \times N}$ to the Rayleigh-fading multipath component, $\kappa_1 \geq 0$ denotes the Rician κ -factor, and β_1 is the large-scale fading coefficient for this link specifically. The large-scale fading coefficient is given by

$$\beta_1 = \frac{\beta_0}{d_{\text{BR}}^{\lambda_{\text{BR}}}}, \quad (5)$$

in which β_0 is the path loss at a reference distance of 1 meter, d_{BR} , and λ_{BR} is the distance and the path-loss exponent between the BS and RIS, respectively. Particularly, the deterministic LoS component can be given through the steering vector of a two-dimensional uniform planar array (UPA). Let us consider the RIS centered in the origin of the Cartesian coordinates; therefore, each column of LoS channel matrix $\bar{\mathbf{H}}_1$ is given as

$$\bar{\mathbf{H}}_1 = \mathbf{a}_B(\vartheta_B) \mathbf{a}_R(\vartheta_R, \varphi_R)^H, \quad (6)$$

where ϑ_B is the azimuthal angle of departure (AoD) of the signal departing from the BS towards the RIS, and ϑ_R and φ_R are the azimuthal and elevation angle of arrival (AoA) at the RIS from the BS. The array response vector of the BS ULA and of the RIS UPA, are defined, respectively as

$$\mathbf{a}_B(\vartheta_B) = \left[1, e^{j\pi \frac{2d_B}{\lambda} \sin \vartheta_B}, \dots, e^{j(M-1)\pi \frac{2d_B}{\lambda} \sin \vartheta_B} \right]^H, \quad (7)$$

$$\begin{aligned} \mathbf{a}_R(\vartheta_R, \varphi_R) &= \left[1, e^{j\pi \frac{2d_R}{\lambda} \sin \vartheta_R \cos \varphi_R}, \dots, e^{j(\sqrt{N}-1)\pi \frac{2d_R}{\lambda} \sin \vartheta_R \cos \varphi_R} \right]^H \\ &\otimes \left[1, e^{j\pi \frac{2d_R}{\lambda} \sin \varphi_R}, \dots, e^{j(\sqrt{N}-1)\pi \frac{2d_R}{\lambda} \sin \varphi_R} \right]^H, \end{aligned} \quad (8)$$

with d_B being the distance between the antenna elements at the BS. Moreover, the multipath component follows an uncorrelated Rayleigh distribution such that $\tilde{\mathbf{h}}_{1,i} \sim \mathcal{CN}(\mathbf{0}_N, \mathbf{I}_N)$, $\forall i \in \{1, \dots, M\}$, with $\tilde{\mathbf{h}}_{1,i}$ being the i -th column of matrix $\tilde{\mathbf{H}}_1$.

RIS-UE link: the link between the RIS and UEs, $\mathbf{H}_2 = [\mathbf{h}_{2,1} \ \mathbf{h}_{2,2} \ \dots \ \mathbf{h}_{2,K}]$, is also assumed to be Rician fading and given as

$$\mathbf{h}_{2,k} = \sqrt{\frac{\beta_{2,k}\kappa_{2,k}}{\kappa_{2,k} + 1}} \bar{\mathbf{h}}_{2,k} + \sqrt{\frac{\beta_{2,k}}{\kappa_{2,k} + 1}} \tilde{\mathbf{h}}_{2,k}, \quad \forall k \in \mathcal{K} \quad (9)$$

where $\bar{\mathbf{h}}_{2,k} \in \mathbb{C}^{N \times 1}$ corresponds to the deterministic LoS channel component between the RIS and the k -th UE, $\tilde{\mathbf{h}}_{2,k} \in \mathbb{C}^{N \times 1}$ to the Rayleigh-fading multipath component between RIS and k -th UE, and $\kappa_{2,k}$ denotes the Rician κ -factor for this same link, with $\kappa_{2,k} \geq 0 \ \forall k \in \mathcal{K}$. Besides, $\beta_{2,k}$ corresponds to the large-scale fading from the RIS to the k -th UE, given as

$$\beta_{2,k} = \frac{\beta_0}{d_{\text{RU},k}^{\lambda_{\text{RU}}}}, \quad (10)$$

with $d_{\text{RU},k}$ being the distance between the RIS and k -th UE, and λ_{RU} the path loss exponent between the RIS and UEs.

LoS Component: similarly to the BS and RIS channel model, the deterministic LoS component $\bar{\mathbf{h}}_{2,k}$ can be given by the steering vector:

$$\begin{aligned} \bar{\mathbf{h}}_{2,k} &= \mathbf{a}_{\text{R},k}(\vartheta_{\text{R},k}, \varphi_{\text{R},k}) \\ &= \left[1, e^{j\pi \frac{2d_{\text{R}}}{\lambda} \sin \vartheta_{\text{R}} \cos \varphi_{\text{R}}}, \dots, e^{j(\sqrt{N}-1)\pi \frac{2d_{\text{R}}}{\lambda} \sin \vartheta_{\text{R}} \cos \varphi_{\text{R}}} \right]^H \otimes \left[1, e^{j\pi \frac{2d_{\text{R}}}{\lambda} \sin \varphi_{\text{R}}}, \dots, e^{j(\sqrt{N}-1)\pi \frac{2d_{\text{R}}}{\lambda} \sin \varphi_{\text{R}}} \right]^H. \end{aligned} \quad (11)$$

B. SE and EE Formulation in RIS-Assisted M-MIMO

In this subsection, we introduce two critical and crucial performance metrics for analyzing the performance of communication systems. We initiate the discussion with the concept of SE and then expand into EE.

1) *Spectral Efficiency:* To assess the wireless system performance, it is crucial to evaluate the capacity for transmitting bits per second per Hertz, namely as SE, a fundamental metric that measures the efficiency of information transmission through a channel. The SE reflects the average number of bits transmitted per channel use across varying fading conditions, serving as a common metric for evaluating communication system capabilities. Since for the RIS-assisted systems, the channel is a generalization of the conventional M-MIMO systems, the SE can be equally represented as the following

$$\text{SE}_k = \log_2(1 + \text{SINR}_k), \quad \left[\frac{\text{bit}}{\text{s} \cdot \text{Hz}} \right] \quad (12)$$

where the signal-to-interference-plus-noise ratio (SINR) of the k -th UE, SINR_k , can be expressed as

$$\text{SINR}_k = \frac{|\mathbf{w}_k^H \mathbf{h}_k|^2}{\sum_{j=1, j \neq K}^K |\mathbf{w}_j \mathbf{h}_k|^2 + |\mathbf{z}^H \Phi \mathbf{h}_{2,k}|^2 + |n_k|^2}. \quad (13)$$

Finally, we can define the system's normalized SR as the following

$$R = \sum_{k=1}^K \log_2 \left(1 + \frac{|\mathbf{w}_k^H \mathbf{h}_k|^2}{\sum_{j=1, j \neq K}^K |\mathbf{w}_j \mathbf{h}_k|^2 + |\mathbf{z}^H \Phi \mathbf{h}_{2,k}|^2 + |n_k|^2} \right). \quad (14)$$

2) *Energy Efficiency*: The metric for evaluating a system's sustainable capacity is referred to as EE. This metric essentially quantifies the number of bits that can be reliably transmitted per unit of energy, expressed as:

$$EE = \frac{\text{Normalized Sum Rate [bit/s/Hz]}}{\text{System Power Consumption [W]}} = \frac{\sum_k SE_k}{P_{\text{total}}} \left[\frac{\text{bit}}{\text{Joule} \cdot \text{Hz}} \right] \quad (15)$$

where P_{total} is the total power consumed by the communication system as detailed in Remark III-B2 and formulated in Subsection III-B3 in the next.

Remark 1 The EE optimization as a function of the amount of transmit RF power in (15) involves a ratio of a convex function in the numerator and an affine function in the denominator. Hence, one can formulate the EE optimization problem as a single-ratio problem, briefly revisited in subsection IV-B.

Remark 2 The power consumption for RIS-assisted M-MIMO systems requires more detailed consideration than traditional M-MIMO systems since although the RIS technology achieves low power consumption, its consumption is not entirely negligible and should be thoroughly examined. Therefore, in the next subsection III-B3 we further detail the adopted system power consumption model.

3) *System's Power Consumption Model*: Different from most prior works, which mostly consider entirely passive RIS, here, we adopt a more practical, realistic energy consumption model by taking into account two primary components: the power consumption of the BS and the power consumption related to the active RIS. Generically, the total power consumption model can be written as

$$P_{\text{total}} = P_{\text{BS}} + P_{\text{RIS}}. \quad (16)$$

The power consumption at the BS is related directly to three main factors: the constant power required for BS operation, *i.e.*, site-cooling, control signaling, load-independent power of backhaul infrastructure, baseband processor, etc; the power necessary to run the circuit components attached to each antenna, such as converters, mixers, filters, etc; and the RF transmit power allocated to the UEs [43], resulting in

$$P_{\text{BS}} = P_{0,\text{BS}} + MP_{\text{M}} + \sum_{k=1}^K \varrho \|\mathbf{w}_k\|^2, \quad (17)$$

where ϱ denotes the inefficiency of the transmit power amplifier.

On the other hand, the RIS needs a controller², which is required for receiving the external signals, processing data, and programming, as well as configuring the RIS unit cells. Overall, the total power consumption dissipated to operate the RIS consists of three parts; **a**) one is the static power consumption generated by the FPGA control board and drive circuits, namely P_{CB} [44], [45]; **b**) the power consumption by the RIS unit cells, being, the power necessary for controlling the impedance of each element via amplifier and phase turner, in order to configure the phase/amplitude of reflection; and **c**) the active power for RF signal amplification. Accordingly, the power consumed at the active RIS can be expressed as

$$P_{\text{RIS}} = P_{\text{CB}} + NP_{\text{N}} + P_{\text{RIS}}^{\text{out}} - P_{\text{RIS}}^{\text{in}}. \quad (18)$$

where $P_{\text{RIS}}^{\text{out}}$ and $P_{\text{RIS}}^{\text{in}}$ is the signal RF power that arrives at the RIS and departs from the RIS, respectively, given by [46]

$$P_{\text{RIS}}^{\text{in}} = \|\mathbf{z}\|^2 + \sum_{k=1}^K \|\mathbf{w}_k^H \mathbf{H}_1\|^2 = \text{tr}(\mathbf{Z}\mathbf{Z}^H) + \sum_{k=1}^K \text{tr}(\mathbf{U}_k \mathbf{U}_k^H), \quad (19)$$

$$P_{\text{RIS}}^{\text{out}} = \|\Phi \mathbf{z}\|^2 + \sum_{k=1}^K \|\mathbf{w}_k^H \mathbf{H}_1 \Phi\|^2 = \text{tr}(\mathbf{Z}\mathbf{v}\mathbf{v}^H \mathbf{Z}^H) + \sum_{k=1}^K \text{tr}(\mathbf{U}_k \mathbf{v}\mathbf{v}^H \mathbf{U}_k^H), \quad (20)$$

²The controller includes a field programmable gate array (FPGA) and drive circuits.

where $\mathbf{Z} \triangleq \text{diag}(z)$ and $\mathbf{U}_k \triangleq \text{diag}(\mathbf{H}_1^H \mathbf{w}_k)$. Thereby, the total RF power amplification at the active RIS can be expressed as

$$\begin{aligned} P_{\text{RIS}}^{\text{out}} - P_{\text{RIS}}^{\text{in}} &= \text{tr}(\mathbf{Z}(\mathbf{v}\mathbf{v}^H - \mathbf{I}_N)\mathbf{Z}^H) + \sum_{k=1}^K \text{tr}(\mathbf{U}_k(\mathbf{v}\mathbf{v}^H - \mathbf{I}_N)\mathbf{U}_k^H) \\ &= \text{tr}((\mathbf{v}\mathbf{v}^H - \mathbf{I}_N)\mathbf{Z}^H\mathbf{Z}) + \text{tr}\left((\mathbf{v}\mathbf{v}^H - \mathbf{I}_N)\sum_{k=1}^K \mathbf{U}_k^H\mathbf{U}_k\right) \\ &= \text{tr}((\mathbf{v}\mathbf{v}^H - \mathbf{I}_K)\mathbf{Q}), \\ &= \mathbf{v}^H\mathbf{Q}\mathbf{v} - \text{tr}(\mathbf{Q}) \end{aligned} \quad (21)$$

where

$$\mathbf{Q} \triangleq \mathbf{Z}^H\mathbf{Z} + \sum_{k=1}^K \mathbf{U}_k^H\mathbf{U}_k \quad (22)$$

Therefore, Eq. (18) also can be written as a function of \mathbf{v} as following³

$$P_{\text{RIS}} = P_{\text{CB}} + NP_{\text{N}} + \mathbf{v}^H\mathbf{Q}\mathbf{v} - \text{tr}(\mathbf{Q}). \quad (23)$$

A detailed discussion on the static power consumption generated by the FPGA board and drive circuits P_{CB} is found in [44], [45].

IV. OPTIMIZATION TECHNIQUES

In order to fully clarify the proposed optimization strategy for tackling the EE active RIS-aided M-MIMO optimization problem, it is crucial to delve into some key optimization techniques that act in our proposed solution. These techniques play essential roles in our approach to addressing the investigated problem, and an entire comprehension of their concepts is essential for a careful understanding of the proposed solution. In the following, we provide a detailed review of these techniques, including LDT and fractional single and multiple-ratio problems.

A. Lagrangian Dual Transform

In addressing the challenge posed by the sum-of-logarithms problem, specific techniques prove to be valuable in easing the management of the optimization problem, thereby enabling the possibility of finding a closed-form, low-complexity solution. Given that communication system-related problems frequently involve logarithmic function summation, finding any form of solution can be exceedingly challenging as the presence of logarithmic functions hinders the analytical tractability and, consequently, optimization. As a result, an optimization technique introduced by [11], namely LDT leverages the Lagrangian duality to externalize the argument of logarithm functions to the outside, eliminating the dependence of the variable of interest with the logarithmic functions, resulting in easier management and analytical tractability of the problem. To further understand the LDT, let us define the following target maximization problem:

$$\begin{aligned} \underset{\mathbf{x}}{\text{maximize}} \quad & \sum_{\ell=1}^L \log\left(1 + \frac{f_{\ell}(\mathbf{x})}{g_{\ell}(\mathbf{x})}\right), \\ \text{subject to} \quad & h_i(\mathbf{x}) \leq 0, \quad i \in \{1, \dots, I\} \end{aligned} \quad (24)$$

$$\text{subject to} \quad h_i(\mathbf{x}) \leq 0, \quad i \in \{1, \dots, I\} \quad (24a)$$

where $f_{\ell}(\mathbf{x}) : \mathbb{C}^N \rightarrow \mathbb{R}_+$ is a non-negative function, and $g_{\ell}(\mathbf{x}) : \mathbb{C}^N \rightarrow \mathbb{R}_+^*$ is a positive function, $\forall \ell \in \{1, \dots, L\}$. It is important to observe that the ratio $f_{\ell}(\mathbf{x})/g_{\ell}(\mathbf{x})$ can have a physical interpretation

³Herein, we assume that the RIS is unable to absorb the incident power, although it is possible by means of energy harvesting circuits embedded at the RIS. Therefore, $P_{\text{RIS}}^{\text{out}} \geq P_{\text{RIS}}^{\text{in}}$ always hold, with the equality when $|v_n| = 1, \forall n \in \mathcal{N}$.

as SINR in our context. The problem (24) is assumed to be a non-convex problem, with a non-convex constraint (24a). According to [12], the problem (24) can be transformed in the following equivalent problem

$$\underset{\mathbf{x}, \boldsymbol{\alpha}}{\text{maximize}} \quad \sum_{\ell=1}^L \log(1 + \gamma_{\ell}) - \sum_{\ell=1}^L \gamma_{\ell} + \sum_{\ell=1}^L (1 + \gamma_{\ell}) \frac{f_{\ell}(\mathbf{x})}{f_{\ell}(\mathbf{x}) + g_{\ell}(\mathbf{x})}, \quad (25)$$

$$\text{subject to} \quad h_i(\mathbf{x}) \leq 0, \quad \forall i \in \{1, \dots, I\} \quad (25a)$$

$$\gamma_{\ell} \geq 0, \quad \forall \ell \in \{1, \dots, L\}. \quad (25b)$$

where $\boldsymbol{\gamma}^{(t)} = [\gamma_1^{(t)}, \gamma_2^{(t)}, \dots, \gamma_L^{(t)}]^T$ is an auxiliary variable, which is iteratively updated, introduced for each ratio term $f_{\ell}(\mathbf{x}^{(t-1)})/g_{\ell}(\mathbf{x}^{(t-1)})$. It's important to note that the two problems, (24) and (25), are equivalent. In other words, at the convergence, the solution \mathbf{x} to (24) is identical to the solution to (25), and their respective optimal objective values are also equal [11, III-B]. Furthermore, it is worth highlighting that, according to the Karush–Kuhn–Tucker (KKT) conditions, we can obtain the following

$$\frac{\partial \left(\sum_{\ell=1}^L \log(1 + \gamma_{\ell}^{(t+1)}) - \sum_{\ell=1}^L \gamma_{\ell}^{(t+1)} + \sum_{\ell=1}^L \frac{(1 + \gamma_{\ell}^{(t+1)})f_{\ell}(\mathbf{x}^{(t)})}{f_{\ell}(\mathbf{x}^{(t)}) + g_{\ell}(\mathbf{x}^{(t)})} \right)}{\partial \gamma_{\ell}} = 0 \quad (26)$$

$$\gamma_{\ell}^{*(t+1)} = \frac{f_{\ell}(\mathbf{x}^{(t)})}{g_{\ell}(\mathbf{x}^{(t)})} \quad (27)$$

This equivalence allows for a seamless transition between the two problem formulations while preserving the optimality.

B. Fractional Programming

Fractional programming theory is the branch of optimization theory concerned with the properties and optimization of fractional functions, *i.e.*, a ratio of two functions that are generally nonlinear. They can be found in several areas and are generically subdivided into two classes: single-ratio problems and multiple-ratio problems. Below, we review techniques designed to address each of these classes and their respective solution methodologies.

Single-Ratio Problems: There are many transforms that deal consistently with this type of problem; the most classical is named *Dinkelbach's Transform* [47], [12], [11]. For a better understanding, let us define the following optimization problem.

$$\underset{\mathbf{x}}{\text{maximize}} \quad \frac{f(\mathbf{x})}{g(\mathbf{x})}, \quad (28)$$

$$\text{subject to} \quad h_i(\mathbf{x}) \leq 0, \quad \forall i \in \{1, \dots, I\} \quad (28a)$$

where $f(\mathbf{x}) : \mathbb{C}^N \rightarrow \mathbb{R}_+$ and $g(\mathbf{x}) : \mathbb{C}^N \rightarrow \mathbb{R}_+$ are non-negative function and positive function, respectively. The conventional approach for dealing with this FP is decoupling the numerator and denominator and treating it jointly. The *Dinkelbach's transform* reformulates the single-ratio problem (28) as the following

$$\underset{\mathbf{x}, \eta}{\text{maximize}} \quad f(\mathbf{x}) - \eta g(\mathbf{x}), \quad (29)$$

$$\text{subject to} \quad h_i(\mathbf{x}) \leq 0, \quad \forall i \in \{1, \dots, I\} \quad (29a)$$

where η is an auxiliary variable that is iteratively updated by

$$\eta^{(t)} = \frac{f(\mathbf{x}^{(t-1)})}{g(\mathbf{x}^{(t-1)})}, \quad (30)$$

where t is the iteration index.

Multiple-Ratio Problems: Although the classic *Dinkelbach's* transform [47] works well for single-ratio problems, they cannot be easily extended to the multiple-ratio problems, since for single-ratio problems, the optimal solution is the same for the original FP and the transformed problem, but not the value of the objective function of both. To solve the multi-ratio problem, several different techniques have been proposed, such as *Quadratic Transform* [11], and [48]. Herein, we focus on the technique developed by [48]. Let us define the following multi-ratio problem:

$$\begin{aligned} & \underset{\mathbf{x}}{\text{maximize}} && \sum_{\ell=1}^L \frac{f_{\ell}(\mathbf{x})}{g_{\ell}(\mathbf{x})}, && (31) \\ & \text{subject to} && h_i(\mathbf{x}) \leq 0, && i \in \{1, \dots, I\} \end{aligned} \quad (31a)$$

where $f_{\ell}(\mathbf{x}) : \mathbb{C}^N \rightarrow \mathbb{R}_+$ and $g_{\ell}(\mathbf{x}) : \mathbb{C}^N \rightarrow \mathbb{R}_+$, $\forall \ell \in \{1, \dots, L\}$. In [48], the authors proposed an iterative solution in order to solve problem (31), where the equivalent problem can be given as

$$\begin{aligned} & \underset{\mathbf{x}, \mathbf{u}, \boldsymbol{\beta}}{\text{maximize}} && \sum_{\ell=1}^L u_{\ell} (f_{\ell}(\mathbf{x}) - \beta_{\ell} g_{\ell}(\mathbf{x})), && (32) \\ & \text{subject to} && h_i(\mathbf{x}) \leq 0, && i \in \{1, \dots, I\} \end{aligned} \quad (32a)$$

where \mathbf{u} and $\boldsymbol{\beta}$ are auxiliary variables which are iteratively updated as

$$u_{\ell}^{(t+1)} = \frac{1}{g_{\ell}(\mathbf{x}^{(t)})}, \quad \forall \ell = 1, \dots, L, \quad (33)$$

$$\beta_{\ell}^{(t+1)} = \frac{f_{\ell}(\mathbf{x}^{(t)})}{g_{\ell}(\mathbf{x}^{(t)})}, \quad \forall \ell = 1, \dots, L. \quad (34)$$

V. PROBLEM FORMULATION

In view of addressing all the aforementioned arguments, with regard to EE exposed in Section I, we formulate an optimization problem whose main objective is optimizing the reflecting coefficients of an active RIS in order to assess the necessary number of RIS elements that should be selected to outperform the entirely passive RIS in terms of EE. The idea is to reduce the number of operating elements in the RIS in view of reducing their power consumption while increasing the total SR by amplifying the incoming signal intended for the UEs. Hence, such an objective can be formulated as the following optimization problem, denoted as \mathcal{P}_0 :

$$\mathcal{P}_0 : \underset{\mathbf{v}}{\text{maximize}} \quad \frac{\sum_{k=1}^K \log_2 \left(1 + \frac{|\mathbf{w}_k^H \mathbf{h}_k|^2}{\sum_{j=1, j \neq k}^K |\mathbf{w}_j \mathbf{h}_k|^2 + |\mathbf{z}^H \boldsymbol{\Phi} \mathbf{h}_{2,k}|^2 + |n_k|^2} \right)}{P_{0,BS} + P_{CB} + M P_M + \sum_{k=1}^K \varrho \|\mathbf{w}_k\|^2 + N P_N + \mathbf{v}^H \mathbf{Q} \mathbf{v} - \text{tr}(\mathbf{Q})}, \quad (35)$$

$$\text{subject to} \quad \text{tr}(\mathbf{Q}) \leq \mathbf{v}^H \mathbf{Q} \mathbf{v} \leq \text{tr}(\mathbf{Q}) + P_{\max}^{\text{RIS}}, \quad (35a)$$

$$|v_n| \leq \alpha_{\max}, \quad \forall n \in \mathcal{N}. \quad (35b)$$

Constraint (35a) considers the maximum amplification of power provided by the active RIS, while constraint (35b) considers the maximum amplitude imposed by each element of the RIS. One should notice that problem \mathcal{P}_0 is more challenging than the EE optimization with entirely passive RIS since the RIS configuration vector also appears in the denominator of the objective function (35).

VI. PROPOSED SOLUTION

In Subsection VI-A, we introduce the proposed algorithm namely FP-based Amplitude/Phase Beamforming Design, which utilizes the FP optimization technique. Specifically, to enhance the convexity of the optimization problem, this algorithm incorporates auxiliary variables derived from Dinkelbach's Transform, LDT, and from the methodology outlined in [48]. This integration strategically molds the objective function into a convex form, facilitating effective optimization.

Subsequently, in Subsection VI-B, we conduct a comprehensive analysis of the algorithm's complexity. This examination provides valuable insights, emphasizing the algorithm's efficiency and suitability for real-world applications.

Finally, in Section VII, we present a comparative evaluation of the proposed algorithm's performance within typical RIS-aided M-MIMO channel and system scenarios. This comparative analysis serves to validate and illustrate the algorithm's efficacy across a range of practical and diverse operating conditions.

A. FP-Based Solution Method

Before delving directly into the problem at hand, it is useful to establish a more concise nomenclature. Therefore, firstly, for the sake of tractability, we shall rewrite Equation (13) as follows

$$\text{SINR}_k = \frac{|\mathbf{w}_k^H \mathbf{h}_k|^2}{\sum_{j=1, j \neq k}^K |\mathbf{w}_j^H \mathbf{h}_k|^2 + |\mathbf{z}^H \Phi \mathbf{h}_{2,k}|^2 + |n_k|^2} = \frac{\mathbf{v}^H \mathbf{A}_k \mathbf{v}}{\mathbf{v}^H \mathbf{B}_k \mathbf{v} + |n_k|^2}, \quad (36)$$

where with few analytical manipulations, we obtain that

$$\mathbf{A}_k \triangleq \mathbf{H}_{2,k}^H \mathbf{H}_1^H \mathbf{w}_k \mathbf{w}_k^H \mathbf{H}_1 \mathbf{H}_{2,k}, \quad (37)$$

$$\mathbf{B}_k \triangleq \mathbf{H}_{2,k}^H \mathbf{z} \mathbf{z}^H \mathbf{H}_{2,k} + \sum_{j=1, j \neq k}^K \mathbf{H}_{2,k}^H \mathbf{H}_1^H \mathbf{w}_j \mathbf{w}_j^H \mathbf{H}_1 \mathbf{H}_{2,k}, \quad (38)$$

with $\mathbf{H}_{2,k} = \text{diag}(\mathbf{h}_{2,k})$. This manipulation enables us to effortlessly address our problem, thereby facilitating the derivation of subsequent equations. Rewriting problem (35), we have the following

$$\begin{aligned} \mathcal{P}_0 : \quad & \underset{\mathbf{v}}{\text{maximize}} \quad \frac{\sum_{k=1}^K \log_2 \left(1 + \frac{\mathbf{v}^H \mathbf{A}_k \mathbf{v}}{\mathbf{v}^H \mathbf{B}_k \mathbf{v} + |n_k|^2} \right)}{\hat{P} + \mathbf{v}^H \mathbf{Q} \mathbf{v}}, \\ & \text{subject to} \quad (35\text{a}), (35\text{b}), \end{aligned} \quad (39)$$

where we define $\hat{P} \triangleq \sum_{k=1}^K \varrho \|\mathbf{w}_k\|^2 + P_{0,\text{BS}} + P_{\text{CB}} + MP_{\text{M}} + NP_{\text{N}} - \text{tr}(\mathbf{Q})$. One can see that Problem (39) is a non-convex problem, with a non-convex constraint (35a). Furthermore, we also should notice that (39) is a single ratio problem. Therefore, prior to solving the optimization process, a pre-processing step should be applied to the objective function due to its intractable fractional form. To decouple the numerator and denominator of (39), we employ the classic Dinkelbach's methodology [47]. Specifically, by introducing an auxiliary variable η , according to subsection IV-B, the original problem can be equivalently reformulated as

$$\begin{aligned} \mathcal{P}_1 : \quad & \underset{\mathbf{v}, \eta}{\text{maximize}} \quad \sum_{k=1}^K \log_2 \left(1 + \frac{\mathbf{v}^H \mathbf{A}_k \mathbf{v}}{\mathbf{v}^H \mathbf{B}_k \mathbf{v} + |n_k|^2} \right) - \eta \left(\hat{P} + \mathbf{v}^H \mathbf{Q} \mathbf{v} \right), \\ & \text{subject to} \quad (35\text{a}), (35\text{b}), \end{aligned} \quad (40)$$

where the optimal η^* in the ℓ -th iteration can be directly computed as

$$\eta^{*\ell} = \frac{\sum_{k=1}^K \log_2 \left(1 + \frac{\mathbf{v}^{(\ell-1)H} \mathbf{A}_k \mathbf{v}^{(\ell-1)}}{\mathbf{v}^{(\ell-1)H} \mathbf{B}_k \mathbf{v}^{(\ell-1)} + \sigma^2} \right)}{\hat{P} + \mathbf{v}^{(\ell-1)H} \mathbf{Q} \mathbf{v}^{(\ell-1)}}. \quad (41)$$

Thus, we should seek to solve \mathcal{P}_1 , for fixed η (at the ℓ -th iteration). In this way, we should see that the objective function of \mathcal{P}_1 is still non-convex. Moreover, it is composed of a scaled version of a multiple-ratio function; therefore, applying the LDT technique, we can introduce the auxiliary variable γ , and rewrite \mathcal{P}_1 in an equivalent way, obtaining the following optimization problem, which we denote as \mathcal{P}_2

$$\begin{aligned} \mathcal{P}_2 : \quad & \underset{\mathbf{v}, \gamma}{\text{maximize}} \quad \sum_{k=1}^K \log_2(1 + \gamma_k) - \gamma_k + \frac{(1 + \gamma_k) \mathbf{v}^H \mathbf{A}_k \mathbf{v}}{(\mathbf{v}^H (\mathbf{A}_k + \mathbf{B}_k) \mathbf{v} + |n_k|^2)} - \eta \left(\hat{P} + \mathbf{v}^H \mathbf{Q} \mathbf{v} \right), \\ & \text{subject to} \quad (35\text{a}), (35\text{b}). \end{aligned}$$

The γ that maximizes \mathcal{P}_2 at the ℓ -th iteration is given by

$$\gamma_k^{*\ell} = \frac{\mathbf{v}^{(\ell-1)H} \mathbf{A}_k \mathbf{v}^{(\ell-1)}}{\mathbf{v}^{(\ell-1)H} \mathbf{B}_k \mathbf{v}^{(\ell-1)} + \sigma^2}, \quad \forall k \in \mathcal{K}. \quad (42)$$

By proceeding, following methodology of [48], and introducing the following auxiliary variables, β , and \mathbf{u} , we can rewrite \mathcal{P}_2 as

$$\begin{aligned} \mathcal{P}'_2 : \quad & \underset{\mathbf{v}, \mathbf{u}, \beta}{\text{maximize}} \quad \sum_{k=1}^K \log_2(1 + \gamma_k) - \gamma_k + u_k \left[(1 + \gamma_k) \mathbf{v}^H \mathbf{A}_k \mathbf{v} - \beta_k (\mathbf{v}^H (\mathbf{A}_k + \mathbf{B}_k) \mathbf{v} + |n_k|^2) \right] \\ & \quad \quad \quad - \eta \left(\hat{P} + \mathbf{v}^H \mathbf{Q} \mathbf{v} \right), \\ & \text{subject to} \quad (35\text{a}), (35\text{b}). \end{aligned} \quad (43)$$

The β_k and u_k that maximize \mathcal{P}'_2 at the ℓ -th iteration can be obtained by the KKT conditions which are given as:

$$\beta_k^{(\ell)*} = \frac{(1 + \gamma_k^{(\ell)}) \mathbf{v}^{(\ell-1)H} \mathbf{A}_k \mathbf{v}^{(\ell-1)}}{\mathbf{v}^{(\ell-1)H} (\mathbf{A}_k + \mathbf{B}_k) \mathbf{v}^{(\ell-1)} + |n_k|^2}, \quad \forall k \in \mathcal{K}, \quad (44)$$

$$u_k^{(\ell)*} = \frac{1}{\mathbf{v}^{(\ell-1)H} (\mathbf{A}_k + \mathbf{B}_k) \mathbf{v}^{(\ell-1)} + |n_k|^2}, \quad \forall k \in \mathcal{K}. \quad (45)$$

Rewriting \mathcal{P}'_2 in a more compact form, we arrive at the following equivalent problem

$$\begin{aligned} \mathcal{P}_3 : \quad & \underset{\mathbf{v}}{\text{maximize}} \quad \mathbf{v}^H \mathbf{C} \mathbf{v}, \\ & \text{subject to} \quad (35\text{a}), (35\text{b}), \end{aligned} \quad (46)$$

where

$$\mathbf{C}^{(\ell)} = -\eta^{(\ell)} \mathbf{Q} + \sum_{k=1}^K u_k^{(\ell)} (1 + \gamma_k^{(\ell)}) \mathbf{A}_k - u_k^{(\ell)} \beta_k^{(\ell)} (\mathbf{A}_k + \mathbf{B}_k). \quad (47)$$

The problem \mathcal{P}_3 can be rewritten in an alternative manner as follows:

$$\mathcal{P}_4 : \quad \underset{\mathbf{V}}{\text{maximize}} \quad \text{tr}(\mathbf{C} \mathbf{V}), \quad (48)$$

$$\text{subject to} \quad \text{tr}(\mathbf{C} \mathbf{V}) \leq \text{tr}(\mathbf{Q}) + P_{\max}^{\text{RIS}}, \quad (48\text{a})$$

$$\text{tr}(\mathbf{C} \mathbf{V}) \geq \text{tr}(\mathbf{Q}) \quad (48\text{b})$$

$$[\mathbf{V}]_{n,n} \leq \alpha_{\max}^2, \quad \forall n \in \mathcal{N} \quad (48\text{c})$$

$$\text{rank}(\mathbf{V}) = 1, \quad (48\text{d})$$

where the $\mathbf{v}^H \mathbf{C} \mathbf{v} = \text{tr}(\mathbf{C} \mathbf{V})$ property is utilized, with $\mathbf{V} = \mathbf{v} \mathbf{v}^H$. In particular, both the objective function and constraints in \mathcal{P}_4 , given by Eq. (48), are linear in the matrix \mathbf{V} [49].

Notice that the constraint (48d) is a non-convex constraint; however, we can relax it in order to obtain a sub-optimal solution for problem \mathcal{P}_4 . In summary, the optimization problem \mathcal{P}_4 can be globally solved by standard fractional programming tools, such as CVX [50]. If the obtained solution of \mathbf{V} has a unit rank, then \mathbf{V} is also feasible for the original problem. Otherwise, a feasible solution can be obtained by randomization techniques [49], [51].

Based on the above derivations, the overall FP-based Amplitude/Phase Beamforming design algorithm is summarized in Algorithm 1. By appropriately initializing the variable \mathbf{v} and the BS transmit power \mathbf{p} , the RIS reflection/amplification matrix $\Phi = \text{diag}(\mathbf{v})$ is iteratively updated, until the EE of the RIS-assisted M-MIMO system converges.

Algorithm 1 FP-based Amplitude/Phase Beamforming Design

Input: \mathbf{p} , \mathbf{A}_k , \mathbf{B}_k , $\forall k \in \{1, \dots, K\}$
Set $\ell = 1$;
Set feasible value for $\mathbf{v}^{(\ell-1)}$;
Set $\eta^{(\ell-1)} = 0$;
repeat
 Step 1: Compute $\eta^{*(\ell)}$ by (41);
 Step 2: Update $\gamma^{*(\ell)}$ by (42);
 Step 3: Compute $\beta^{*(\ell)}$ by (44);
 Step 4: Update $\mathbf{u}^{*(\ell)}$ by (45);
 Step 5: Obtain $\mathbf{v}^{(\ell)}$ by solving \mathcal{P}_4 ;
 Step 6: $\ell = \ell + 1$;
until $|\eta^{*(\ell)} - \eta^{*(\ell-1)}| < \epsilon$
Output: $\mathbf{v}^* = [\alpha_1^* e^{-j\theta_1^*}, \alpha_2^* e^{-j\theta_2^*}, \dots, \alpha_N^* e^{-j\theta_N^*}]^H$

B. Complexity

So far, we have completed the design of active RIS phase shift matrix Φ . For clarity of this scheme procedure, we summarize the main ideas of the entire proposed FP-based amplitude/phase beamforming design algorithm as follows. First, by fixing η , we can obtain γ , β , and \mathbf{u} , with closed-form expressions, and the RIS phase-shift matrix \mathbf{v} by solving \mathcal{P}_4 , as illustrated on Algorithm 1. The alternating iterating procedure is repeated among four variables until the termination condition is reached. Herein, we describe the complexity of the proposed iterative algorithm. It is known that, the complexity to update γ , β , \mathbf{u} , and solving \mathcal{P}_4 are $\mathcal{O}(2KN^2)$, $\mathcal{O}(2KN^2)$, $\mathcal{O}(KN^2)$, and $\mathcal{O}(N^2)$ [49] respectively. Besides, the η updating requires $\mathcal{O}(3KN^2)$. Therefore, the overall complexity is given by $\mathcal{O}(8LKN^2 \ln(\frac{1}{\epsilon}))$ Floating Point Operations (FLOPs), where L denotes the number of loop iterations. In addition, it is worthy to notice that the complexity of the Gaussian randomization method is of $\mathcal{O}(N^2)$ per draw [52].

VII. NUMERICAL RESULTS

Herein, in this section we illustrate simulation results in view to demonstrate the effectiveness of the proposed FP-based amplitude/phase beamforming design algorithm, where the active RIS amplitude/phase vector is obtained by running Algorithm 1, where we solve \mathcal{P}_4 via convex optimization with CVX solver, in MATLAB. For the simulation setup, we assume that the UEs are positioned in a circle with a radius of 10 m from the center (30 m, 30 m), the BS is located at (-10 m, 5 m) and the RIS is located at the origin (0 m, 0 m). For the BSRIS link, we defined $\beta_0^{\text{BR}} = 1e^{-3}$ and $\lambda^{\text{BR}} = 2$, while for the RIS-UEs link, we assume $\beta_0^{\text{RU}} = 1e^{-3}$ and $\lambda^{\text{RU}} = 2.5$. Unless specified otherwise, the remainder of the parameters are listed in Table II. Aiming for a fair comparison, we assume the same power budget for entirely passive RIS and active RIS, where the maximum power for RIS amplification, $P_{\text{max}}^{\text{RIS}}$, is given by $P_{\text{max}}^{\text{RIS}} = \tau_{\text{RIS}} P_{\text{TX}}$, where $\tau_{\text{RIS}} \in [0, 1]$.

TABLE II
LIST OF SIMULATION PARAMETERS.

Parameter	Description
$P_{\text{TX}} = [10 : 5 : 50]$ dBm	Maximum power budget at BS
$\sigma_k^2 = -95$ dBm	Noise variance at UEs, $\forall k \in \mathcal{K}$
$\sigma_{\text{RIS}}^2 = -80$ dBm	Noise variance at RIS
$K = 5$	Numbers of UEs
$M = 32$	Number of antennas at BS
$N = 64$	Number of reflecting meta-surfaces elements
$\varrho = 1.2$	Power amplifier inefficiency
$P_{0,\text{BS}} = 9$ dBW	Fixed power consumption at BS
$P_{\text{M}} = 1$ W	Power consumed by a BS transceiver chain
$P_{\text{CB}} = 4.8$ W	Power consumed by control board
$P_{\text{N}} = 10$ dBm	Power of RIS element configuration
$\alpha_{\text{max}} = 10$	Maximum amplitude gain
$\kappa_1 = 0.1$	Rician coefficient for BS RIS link
$\kappa_{2,k} = 0.01$	Rician coefficient for RIS UEs links, $\forall k \in \mathcal{K}$
$\tau_{\text{RIS}} = 0.15$	Coefficient for RIS amplification
$\mathcal{T} = 500$	Realizations Monte-Carlo Simulation (MCs)

A. Energy Efficiency vs. Transmit Power Budget

Initially, in Fig. 1, we assess and compare the EE of both RIS architecture as a function of transmit power P_{TX} . For each point in the curve, the proposed algorithm is employed to optimize the power of reflection of the active RIS array, while for the passive RIS we just optimize the phase shift angles. We denote as ‘‘Passive RIS’’ the entirely passive RIS, ‘‘Active RIS’’ the active RIS, ‘‘Random RIS’’ as the entirely passive RIS with random precoding and random RIS reflecting coefficients matrix.

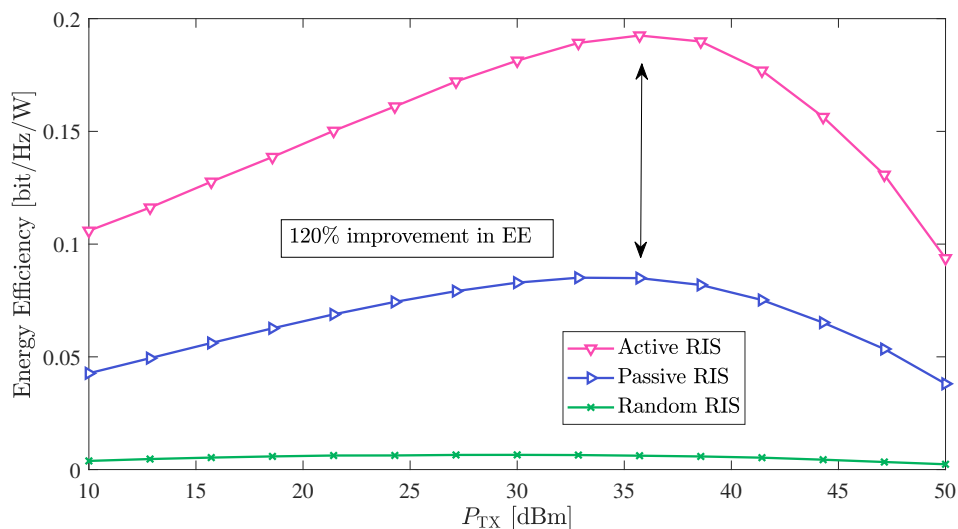


Fig. 1. Average EE vs the transmit power budget [dBm] at the BS (P_{TX}). Performance evaluation of the proposed algorithm for the active RIS vs entirely passive RIS and random phase shift/precoding, with $N = 25$.

We can first observe the considerable impact that both passive and active RIS can exert on the system performance, particularly in terms of EE. This emphasizes the critical importance of optimizing both precoding and the matrix of reflecting coefficients of the RIS within the RIS-aided M-MIMO scenario since it can deal with the interference, improving the system SE, and consequently the system EE. Furthermore,

delving deeper into our findings, the result reveals that the proposed active RIS optimization method significantly improves the EE of the RIS-assisted M-MIMO system compared to the entirely passive RIS configuration. Specifically, our result indicates that the active RIS can outperform the performance of its entirely passive counterpart, achieving an impressive improvement of up to 120% in the peak value at ≈ 36 dBm. This emphasizes the efficacy of deploying active RIS in maximizing the EE, demonstrating its ability to deal with the double-fading attenuation drawback significantly.

B. Percentage of Amplification Power Utilized

Figure 2 illustrates the percentage of utilized amplification power as a function of the number of reflecting elements for two distinct strategies: 1) SR maximization, and 2) maximization of EE. One can see through this result that amplification power P_{\max}^{RIS} increases as the number of reflecting elements increases. A reason for such a behavior is that when N is low, utilizing fully P_{\max}^{RIS} can result in higher interference, and consequently poor EE since the denominator of (35) also increases with P_{\max}^{RIS} . Besides, by increasing the number of reflecting elements, the RIS can easily achieve equality on the right side of constraint (35a), showing that as higher is N , better the RIS can manage the interference. Furthermore, one can see that the utilized power amplification for the SR maximization strategy is also limited for scenarios when N assumes low values, confirming that this power management is necessary for the optimization of both metrics.

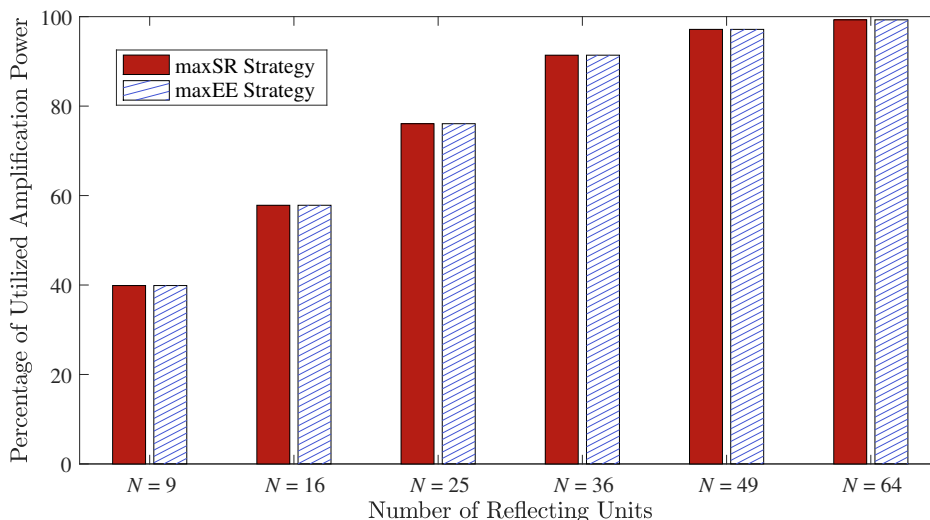


Fig. 2. Percentage of power amplification utilized vs the number of reflecting elements for the proposed algorithm. In this setup, we set $P_{\text{TX}} = 35$ dBm.

In Figure 3, we plot the cumulative density function (CDF) of the *average amplitude gain* of the active RIS, $\bar{\alpha} = \frac{1}{N} \sum_{n=1}^N \alpha_n$, for some values of $N \in [9; 64]$ RIS elements. One can observe that the probability of $\bar{\alpha}$ to assume a low value, is higher for $N = 9$, than $N = [16, 25, 36, 49, 64]$. This coincides with the result shown in Fig. 2, justifying the fact that low N values ($N = \{9, 16\}$) utilize lower amplification power. However, for $N = 64$, the algorithm also applies low values of $\bar{\alpha}$. This is because, within scenarios where N assumes high values, the maximum available amplification power is easily achieved. We can see that by increasing N from $N = 49$, the $\bar{\alpha}$ value starts to decrease.

C. Number of RIS Reflecting Elements

In the sequel, Fig. 4 illustrates the system EE as a function of the number of reflecting elements (N) of RIS. Additionally, the performance of an entirely passive RIS, with a fixed number of elements $N = 64$, is depicted in the plot. We can see that the active RIS exhibits comparable performance to the

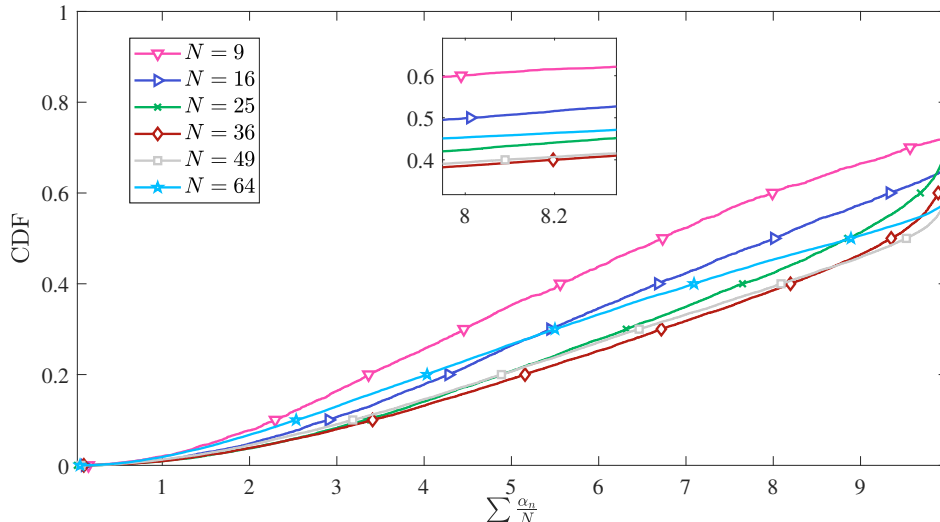


Fig. 3. CDF of the average value of amplitude obtained with the proposed algorithm. Here we set $P_{\text{TX}} = 35$ dBm.

passive RIS when equipped with ≈ 23 reflecting elements. In other words, an active RIS with $N = 25$ ($N_v = N_h = 5$) can surpass, in terms of EE, the entirely passive RIS-aided M-MIMO with $N = 64$ elements. Furthermore, we can see when we increase the number of UEs K , the number of RIS elements is slightly affected. This again demonstrates the potential of amplifying the incoming signal at the RIS, enabling the possibility of reducing the number of elements on the RIS without compromising the system EE performance. Additionally, it shows the potential of active RIS to reduce the channel estimation overhead, keeping the same performance as entirely passive RIS, which can be very useful for practical systems since the channel estimation overhead is one of the most critical drawbacks associated with the RIS technology.

This unveils an interesting aspect of the active RIS, that enables it to achieve the same EE performance as passive RIS while reducing the size of the array physically. Let's assume elements with a size of $d = \lambda$ and an adjacent spacing between elements of $d_R = \frac{\lambda}{2}$. For a frequency operation of $f = 5$ GHz, where the wavelength is $\lambda = 60$ mm, the length of RIS can be calculated using the formula $\mathcal{L} = \lambda N_h + \frac{\lambda(N_h-1)}{2}$. With $N = 64$, the length is $\mathcal{L} = 69$ cm, while for active RIS with $N = 25$ the length is 42 cm. This demonstrates that the active RIS can achieve comparable performance with a physically smaller array, providing potential deployment advantages.

Moreover, envisioning a scenario where system priorities may shift between SE or EE metrics, a dynamic approach to controlling the number of active RIS elements becomes paramount. For instance, when the SE is the priority, employing a higher quantity of operating elements is a natural choice. However, when prioritizing EE, a conscious reduction in the number of acting elements becomes crucial. This flexibility allows an opportunistic and consistent selection of RIS elements conditioned to the system's specific needs in different operational contexts.

D. Convergence Performance of Proposed Algorithm

Fig. 5 illustrates the convergence behavior of the proposed algorithm under various conditions, showcasing their effectiveness for each one. The monotonic convergence patterns are examined across three distinct values of P_{TX} with constant N , and for the same P_{TX} under two different values of N . It is clear that the EE initially experiences an upward trend and subsequently stabilizes with increasing iterations across all modes, highlighting the efficiency of the proposed algorithm. In addition, a noteworthy trend can be observed: as the number of reflective elements N increases, so does the achieved EE. Moreover, we can see that the proposed algorithm demonstrates rapid convergence (number of iterations) since it does not need many iterations (6 to 9 iterations) to converge, *e.g.*, for the case when $P_{\text{TX}} = 35$, and $N = 64$,

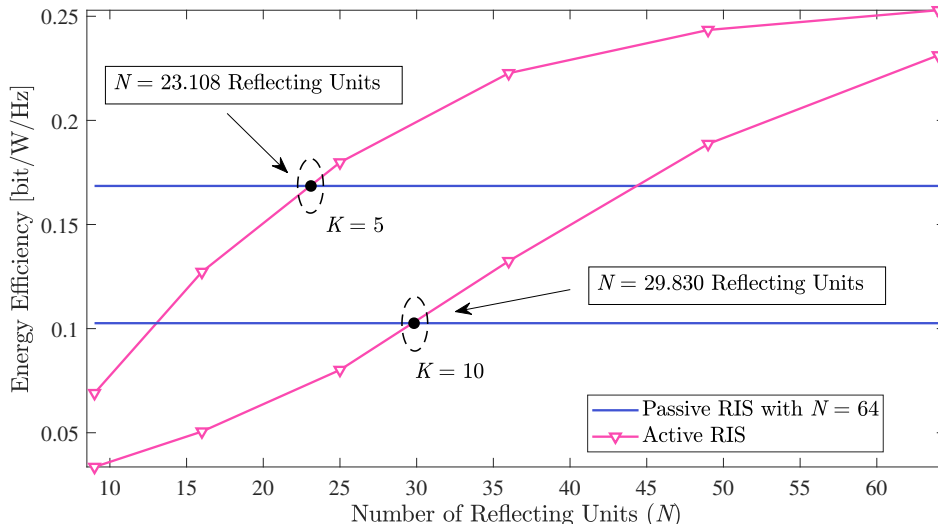


Fig. 4. Average EE vs number of RIS reflecting units. Performance evaluation of the proposed algorithm for the active RIS vs entirely passive RIS with fixed number of elements $N = 64$, for $P_{TX} = 35$ dBm and two different number of UEs, $K = 5$ and $K = 10$.

the number of iteration necessary to converge is 6, while for $P_{TX} = 50$, and $N = 25$, the number of iteration necessary to converge is 9. This result shows that the power level has a more significant impact on convergence than the number of reflective elements, providing valuable insights into the algorithm's efficiency under varying operational conditions.

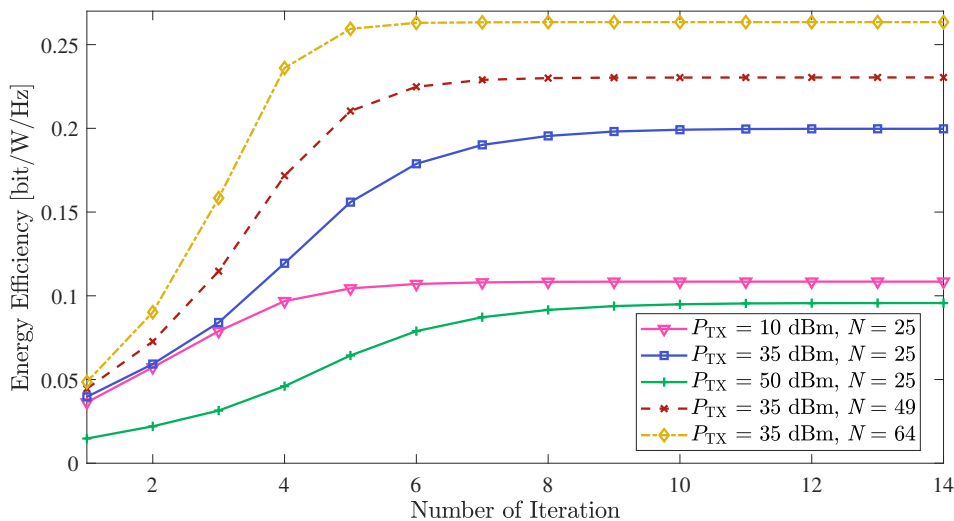


Fig. 5. Average EE vs number of iterations for the proposed algorithm. Performance evaluation of the proposed algorithm for the active RIS with fixed number of elements $N = 25$, for $P_{TX} = \{10, 35, 50\}$ dBm and for fixed transmit power budget $P_{TX} = 35$ dBm and $N = \{49, 64\}$.

VIII. CONCLUSIONS

We have examined the profound implications of optimizing the EE for active RIS scenarios, seeking to understand and find the number of elements that need to be selected for acting in active RIS given outperforming its entirely passive RIS counterpart. By exploring various optimization techniques, we aim to provide a low-complexity solution and ensure its proximity to the optimal solution. This approach allows us to assess the effectiveness of our analytical methodology to handle complex optimization challenges.

The numerical results show that the active RIS can easily outperform the entirely passive RIS in terms of system EE, achieving a gain of about 120%. Furthermore, for typical system and channel scenarios, active RIS can operate with less than half of elements compared with the passive RIS in view of achieving about the same performance, enabling an operational cost reduction for physical arrays and lower channel estimation overhead for practical implementations. However, to achieve better performance in signal amplification, the active RIS needs to be equipped with a reasonable number of reflective elements, mainly in scenarios where the available power for signal amplification is high. Finally, we show how the proposed algorithm can be promising since it has required a few iterations for convergence.

We delved into the optimization of energy efficiency (EE) in RIS-assisted M-MIMO systems. While significant progress has been made, several crucial aspects pose open research challenges, offering promising avenues for exploration. Our initial focus was on optimizing the RIS reflection coefficients within the framework of MR precoding with EPA. However, it is noteworthy that the precoding strategy at the BS also presents an opportunity for optimization. Considering the joint optimization of RIS and BS precoding can potentially unveil enhanced EE performance.

Moreover, our system model has assumed a far-field propagation channel. Extending and investigating the analysis of near-field propagation channels is a very relevant topic for future works. This extension is particularly pertinent due to the prevalence of large aperture arrays aimed at mitigating the multiplicative path-loss effect, and higher frequency operations for increased bandwidth, which inherently increase the Rayleigh distance. Notably, this has extended the range where near-field propagation dominates. Furthermore, new opportunities arise in the near-field context; for instance, the beam-focusing effect becomes a prominent phenomenon. This effect not only allows adjustment of the direction of the reflected beam but also offers the intriguing capability to control the distance within a specific angle. Developing strategies to improve the EE of RIS-assisted M-MIMO networks leveraging the beam-focusing effect for near-field scenarios is thus of significant relevance.

Additionally, the current investigation centered on a single active RIS. Extending the system model to accommodate a scenario with multiple active RIS units is a valuable avenue for future research, offering insights into the complexities and opportunities associated with such configurations.

Finally, the optimization scope can be broadened by considering the joint optimization of BS and RIS antenna elements. By optimizing both components simultaneously, the overall EE of the system can be finely tuned for improved performance and resource utilization. These avenues highlight the richness of potential research directions in advancing the understanding and optimization of active RIS-assisted M-MIMO systems.

REFERENCES

- [1] Q. Wu and R. Zhang, "Towards Smart and Reconfigurable Environment: Intelligent Reflecting Surface Aided Wireless Network," *IEEE Communications Magazine*, vol. 58, no. 1, pp. 106–112, 2020.
- [2] S. Gong, X. Lu, D. T. Hoang, D. Niyato, L. Shu, D. I. Kim, and Y.-C. Liang, "Toward Smart Wireless Communications via Intelligent Reflecting Surfaces: A Contemporary Survey," *IEEE Communications Surveys and Tutorials*, vol. 22, no. 4, pp. 2283–2314, 2020.
- [3] A. Taha, M. Alrabeiah, and A. Alkhateeb, "Enabling Large Intelligent Surfaces With Compressive Sensing and Deep Learning," *IEEE Access*, vol. 9, pp. 44 304–44 321, 2021.
- [4] R. Long, Y.-C. Liang, Y. Pei, and E. G. Larsson, "Active Reconfigurable Intelligent Surface-Aided Wireless Communications," *IEEE Transactions on Wireless Communications*, vol. 20, no. 8, pp. 4962–4975, 2021.
- [5] J. An, C. Yuen, L. Dai, M. D. Renzo, M. Debbah, and L. Hanzo, "Toward Beamfocusing-Aided Near-Field Communications: Research Advances, Potential, and Challenges," 2023.
- [6] X. Zhang and H. Zhang, "Hybrid Reconfigurable Intelligent Surfaces-Assisted Near-Field Localization," *IEEE Communications Letters*, vol. 27, no. 1, pp. 135–139, 2023.
- [7] Z. Wu and L. Dai, "Multiple Access for Near-Field Communications: SDMA or LDMA?" *IEEE Journal on Selected Areas in Communications*, vol. 41, no. 6, pp. 1918–1935, 2023.
- [8] I. Ahmed, M. K. Shahid, H. Khammari, and M. Masud, "Machine Learning Based Beam Selection With Low Complexity Hybrid Beamforming Design for 5G Massive MIMO Systems," *IEEE Transactions on Green Communications and Networking*, vol. 5, no. 4, pp. 2160–2173, 2021.
- [9] T. Huang, W. Yang, J. Wu, J. Ma, X. Zhang, and D. Zhang, "A Survey on Green 6G Network: Architecture and Technologies," *IEEE Access*, vol. 7, pp. 175 758–175 768, 2019.
- [10] Y. Liu, Z. Wang, J. Xu, C. Ouyang, X. Mu, and R. Schober, "Near-Field Communications: A Tutorial Review," *IEEE Open Journal of the Communications Society*, vol. 4, pp. 1999–2049, 2023. [Online]. Available: <https://doi.org/10.1109%2Fofcoms.2023.3305583>

- [11] K. Shen and W. Yu, "Fractional Programming for Communication Systems—Part II: Uplink Scheduling via Matching," *IEEE Transactions on Signal Processing*, vol. 66, no. 10, pp. 2631–2644, 2018.
- [12] —, "Fractional Programming for Communication Systems—Part I: Power Control and Beamforming," *IEEE Transactions on Signal Processing*, vol. 66, no. 10, pp. 2616–2630, 2018.
- [13] H. Guo, Y.-C. Liang, J. Chen, and E. G. Larsson, "Weighted Sum-Rate Maximization for Reconfigurable Intelligent Surface Aided Wireless Networks," *IEEE Transactions on Wireless Communications*, vol. 19, no. 5, pp. 3064–3076, 2020.
- [14] C. Pan, H. Ren, K. Wang, W. Xu, M. Elkashlan, A. Nallanathan, and L. Hanzo, "Multicell MIMO Communications Relying on Intelligent Reflecting Surfaces," *IEEE Transactions on Wireless Communications*, vol. 19, no. 8, pp. 5218–5233, 2020.
- [15] K. Zhi, C. Pan, H. Ren, and K. Wang, "Ergodic Rate Analysis of Reconfigurable Intelligent Surface-Aided Massive MIMO Systems With ZF Detectors," *IEEE Communications Letters*, vol. 26, no. 2, pp. 264–268, 2022.
- [16] M. Zeng, E. Bedeer, O. A. Dobre, P. Fortier, Q.-V. Pham, and W. Hao, "Energy-Efficient Resource Allocation for IRS-Assisted Multi-Antenna Uplink Systems," *IEEE Wireless Communications Letters*, vol. 10, no. 6, pp. 1261–1265, 2021.
- [17] W. de Souza and T. Abrão, "Energy Efficiency Maximization for Intelligent Surfaces Aided Massive MIMO With Zero Forcing," *IEEE Transactions on Green Communications and Networking*, pp. 1–1, 2023.
- [18] Z. Li, J. Zhang, J. Zhu, and L. Dai, "RIS Energy Efficiency Optimization with Practical Power Models," in *2023 International Wireless Communications and Mobile Computing (IWCMC)*, 2023, pp. 1172–1177.
- [19] Y. He, Y. Cai, H. Mao, and G. Yu, "RIS-Assisted Communication Radar Coexistence: Joint Beamforming Design and Analysis," *IEEE Journal on Selected Areas in Communications*, vol. 40, no. 7, pp. 2131–2145, July 2022.
- [20] J. Kang, H. Wymeersch, C. Fischione, G. Seco-Granados, and S. Kim, "Optimized Switching Between Sensing and Communication for mmWave MU-MISO Systems," in *2022 IEEE International Conference on Communications Workshops (ICC Workshops)*, 2022, pp. 498–503.
- [21] J. Wu, S. Kim, and B. Shim, "Energy-Efficient Power Control and Beamforming for Reconfigurable Intelligent Surface-Aided Uplink IoT Networks," *IEEE Transactions on Wireless Communications*, vol. 21, no. 12, pp. 10 162–10 176, 2022.
- [22] T. Ji, M. Hua, C. Li, Y. Huang, and L. Yang, "Robust Max-Min Fairness Transmission Design for IRS-Aided Wireless Network Considering User Location Uncertainty," *IEEE Transactions on Communications*, vol. 71, no. 8, pp. 4678–4693, 2023.
- [23] H. Xie, J. Xu, and Y.-F. Liu, "Max-Min Fairness in IRS-Aided Multi-Cell MISO Systems With Joint Transmit and Reflective Beamforming," *IEEE Transactions on Wireless Communications*, vol. 20, no. 2, pp. 1379–1393, 2021.
- [24] T. Jiang and W. Yu, "Interference Nulling Using Reconfigurable Intelligent Surface," *IEEE Journal on Selected Areas in Communications*, vol. 40, no. 5, pp. 1392–1406, 2022.
- [25] J. V. Alegría and F. Rusek, "Channel Orthogonalization with Reconfigurable Surfaces," in *2022 IEEE Globecom Workshops (GC Wkshps)*, 2022, pp. 37–42.
- [26] M. Liu, H. Ren, C. Pan, B. Wang, Z. Yu, R. Weng, K. Zhi, and Y. He, "Joint Beamforming Design for Double Active RIS-assisted Radar-Communication Coexistence Systems," 2024.
- [27] S. Zargari, A. Hakimi, C. Tellambura, and S. Herath, "Multiuser MISO PS-SWIPT Systems: Active or Passive RIS?" *IEEE Wireless Communications Letters*, vol. 11, no. 9, pp. 1920–1924, 2022.
- [28] Z. Zhang, L. Dai, X. Chen, C. Liu, F. Yang, R. Schober, and H. V. Poor, "Active RIS vs. Passive RIS: Which Will Prevail in 6G?" *IEEE Transactions on Communications*, vol. 71, no. 3, pp. 1707–1725, 2023.
- [29] J. Ye, M. Rihan, P. Zhang, L. Huang, S. Buzzi, and Z. Chen, "Energy Efficiency Optimization in Active Reconfigurable Intelligent Surface-Aided Integrated Sensing and Communication Systems," 2023.
- [30] W. Lv, J. Bai, Q. Yan, and H. M. Wang, "RIS-Assisted Green Secure Communications: Active RIS or Passive RIS?" *IEEE Wireless Communications Letters*, vol. 12, no. 2, pp. 237–241, 2023.
- [31] J. H. I. de Souza, J. C. M. Filho, A. Amiri, and T. Abrão, "QoS-Aware User Scheduling in Crowded XL-MIMO Systems Under Non-Stationary Multi-State LoS/NLoS Channels," *IEEE Transactions on Vehicular Technology*, vol. 72, no. 6, pp. 7639–7652, 2023.
- [32] H. L. dos Santos, J. C. Marinello, C. M. Panazio, and T. Abrão, "Machine learning-aided pilot and power allocation in multi-cellular massive MIMO networks," *Physical Communication*, vol. 52, p. 101646, 2022. [Online]. Available: <https://www.sciencedirect.com/science/article/pii/S1874490722000295>
- [33] J. C. M. Filho, G. Brante, R. D. Souza, and T. Abrão, "Exploring the Non-Overlapping Visibility Regions in XL-MIMO Random Access and Scheduling," *IEEE Transactions on Wireless Communications*, vol. 21, no. 8, pp. 6597–6610, 2022.
- [34] J. H. Inacio de Souza, J. C. Marinello Filho, T. Abrão, and C. Panazio, "Reconfigurable Intelligent Surfaces to Enable Energy-Efficient IoT Networks," in *2022 Symposium on Internet of Things (SIoT)*, 2022, pp. 1–4.
- [35] J. C. Marinello, T. Abrão, A. Amiri, E. de Carvalho, and P. Popovski, "Antenna Selection for Improving Energy Efficiency in XL-MIMO Systems," *IEEE Transactions on Vehicular Technology*, vol. 69, no. 11, pp. 13 305–13 318, 2020.
- [36] L. M. Taniguchi, J. H. I. de Souza, D. W. M. Guerra, and T. Abrão, "Resource Efficiency and Pilot Decontamination in XL-MIMO Double-Scattering Correlated Channels," *Transactions on Emerging Telecommunications Technologies*, vol. 32, no. 12, p. e4365, 2021. [Online]. Available: <https://onlinelibrary.wiley.com/doi/abs/10.1002/ett.4365>
- [37] G. A. Ubiali, J. C. Marinello, and T. Abrão, "Energy-efficient Flexible and Fixed Antenna Selection Methods for XL-MIMO Systems," *AEU-International Journal of Electronics and Communications*, vol. 130, p. 153568, 2021.
- [38] J. C. M. Filho, T. Abrão, E. Hossain, and A. Mezghani, "Reconfigurable Intelligent Surfaces-Enabled Intra-Cell Pilot Reuse in Massive MIMO Systems," *IEEE Transactions on Wireless Communications*, pp. 1–1, 2024.
- [39] K. B. Rosa and T. Abrão, "Improving the Resource Efficiency in Massive MIMO-NOMA Systems," *Journal of Network and Systems Management*, vol. 31, no. 4, p. 74, 2023.
- [40] Q. Wu and R. Zhang, "Intelligent Reflecting Surface Enhanced Wireless Network via Joint Active and Passive Beamforming," *IEEE Transactions on Wireless Communications*, vol. 18, no. 11, pp. 5394–5409, 2019.
- [41] C. You, B. Zheng, and R. Zhang, "Fast Beam Training for IRS-Assisted Multiuser Communications," *IEEE Wireless Communications Letters*, vol. 9, no. 11, pp. 1845–1849, 2020.

- [42] L. Jiang, X. Li, M. Matthaiou, and S. Jin, "Joint User Scheduling and Phase Shift Design for RIS Assisted Multi-Cell MISO Systems," *IEEE Wireless Communications Letters*, vol. 12, no. 3, pp. 431–435, 2023.
- [43] E. Björnson, L. Sanguinetti, J. Hoydis, and M. Debbah, "Optimal Design of Energy-Efficient Multi-User MIMO Systems: Is Massive MIMO the Answer?" *IEEE Transactions on Wireless Communications*, vol. 14, no. 6, pp. 3059–3075, 2015.
- [44] J. Wang, W. Tang, J. C. Liang, L. Zhang, J. Y. Dai, X. Li, S. Jin, Q. Cheng, and T. J. Cui, "Reconfigurable Intelligent Surface: Power Consumption Modeling and Practical Measurement Validation," 2024.
- [45] X. Pei, H. Yin, L. Tan, L. Cao, Z. Li, K. Wang, K. Zhang, and E. Bjornson, "RIS-Aided Wireless Communications: Prototyping, Adaptive Beamforming, and Indoor/Outdoor Field Trials," *IEEE Transactions on Communications*, vol. 69, no. 12, p. 8627–8640, Dec. 2021. [Online]. Available: <http://dx.doi.org/10.1109/TCOMM.2021.3116151>
- [46] R. K. Foteck, A. Zappone, and M. D. Renzo, "Energy Efficiency in RIS-Aided Wireless Networks: Active or Passive RIS?" 2023.
- [47] W. Dinkelbach, "On Nonlinear Fractional Programming," *Manage. Sci.*, vol. 133, no. 7, pp. 492–498, 1967.
- [48] Y. Jong, "An Efficient Global Optimization Algorithm for Nonlinear Sum-of-Ratios Problem," *Optimization Online*, 2012.
- [49] Z.-q. Luo, W.-k. Ma, A. M.-c. So, Y. Ye, and S. Zhang, "Semidefinite Relaxation of Quadratic Optimization Problems," *IEEE Signal Processing Magazine*, vol. 27, no. 3, pp. 20–34, 2010.
- [50] M. Grant and S. Boyd, "CVX: Matlab software for disciplined convex programming, version 2.1," <https://cvxr.com/cvx>, Mar. 2014.
- [51] Y. Xu, H. Xie, Q. Wu, C. Huang, and C. Yuen, "Robust Max-Min Energy Efficiency for RIS-Aided HetNets With Distortion Noises," *IEEE Transactions on Communications*, vol. 70, no. 2, pp. 1457–1471, 2022.
- [52] N. Sidiropoulos and Z.-Q. Luo, "A Semidefinite Relaxation Approach to MIMO Detection for High-Order QAM Constellations," *IEEE Signal Processing Letters*, vol. 13, no. 9, pp. 525–528, 2006.